

Reconstruction of an InAs nanowire using geometric and algebraic tomography

R S Pennington¹, S König², A Alpers², C B Boothroyd¹ and R E Dunin-Borkowski^{3,1}

¹ Center for Electron Nanoscopy, Technical University of Denmark, DK-2800 Kongens Lyngby, Denmark

² Zentrum Mathematik, Technische Universität München, Boltzmannstr. 3, D-85747 Garching bei München, Germany

³ Ernst Ruska-Centre for Microscopy and Spectroscopy with Electrons, Forschungszentrum Jülich, D-52425 Jülich, Germany

E-mail: rp@cen.dtu.dk

Abstract. Geometric tomography and conventional algebraic tomography algorithms are used to reconstruct cross-sections of an InAs nanowire from a tilt series of experimental annular dark-field images. Both algorithms are also applied to a test object to assess what factors affect the reconstruction quality. When using the present algorithms, geometric tomography is faster, but artifacts in the reconstruction may be difficult to recognize.

1. Introduction

Conventional algebraic tomography reconstruction algorithms such as the simultaneous iterative reconstruction technique (SIRT) [1] reconstruct a three-dimensional object of varying density from a tilt series of projected images. In contrast, geometric tomography (GT) [2] reconstructs only the shape of the object, using additional information such as e.g. convexity, if applicable.

Here, we reconstruct the cross-section of an InAs nanowire from a tilt series of experimental annular dark-field images using a GT algorithm [3], and compare to the results from a conventional SIRT reconstruction. Additional comparisons using a simulated test object are used to assess the fidelity of each reconstruction and the ease with which artifacts can be identified.

2. Conventional algebraic reconstruction

A high-angle annular dark-field scanning transmission electron microscopy (HAADF STEM) image series of an InAs nanowire was acquired using a probe-aberration-corrected FEI Titan 80-300 operated at 300 kV with a probe convergence semi-angle of 18 mrad and an inner detector semi-angle of 100 mrad. The images were acquired over a total angular range of 139° with a 1° tilt increment. The original 2048×2048 pixel images were then binned by a factor of 4 to reduce noise in the reconstruction. A bright-field TEM image of the nanowire and two representative HAADF STEM images and line profiles from the tilt series are shown in Fig. 1.

SIRT reconstruction was performed using the TomoJ software with 15 iterations [4, 5] after aligning the original tilt series using cross-correlation and a Canny-Deriche edge-detection filter.

Cross-sections of the wire determined from reconstructions using 14 and 140 projections are shown in Fig. 2 and Fig. 3, respectively, for both of the sections of the nanowire marked in Fig. 1.

The SIRT reconstruction is blurred in the direction of the “missing wedge”, contains artifacts in the region outside the wire, and requires a subjective choice of threshold to find the nanowire boundary.

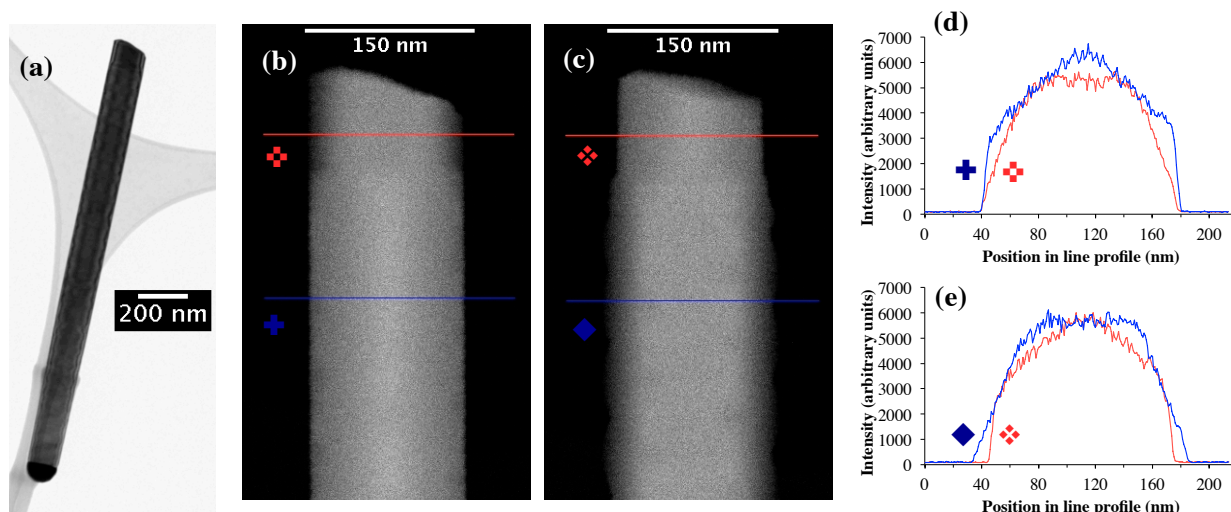


Figure 1. (a) is a bright-field TEM image of the InAs nanowire specimen used for tomography; (b) and (c) aligned binned HAADF STEM images taken from the tilt series of the wire at angles of 7° and 37° , respectively, with 8-pixel-wide line profiles from the marked regions shown in (d) and (e), exhibiting the roughly-hexagonal faceting expected from the reconstruction, but not noise levels. There is a growth defect between the red and blue line profile, leading to rotation in the blue profile relative to the red.

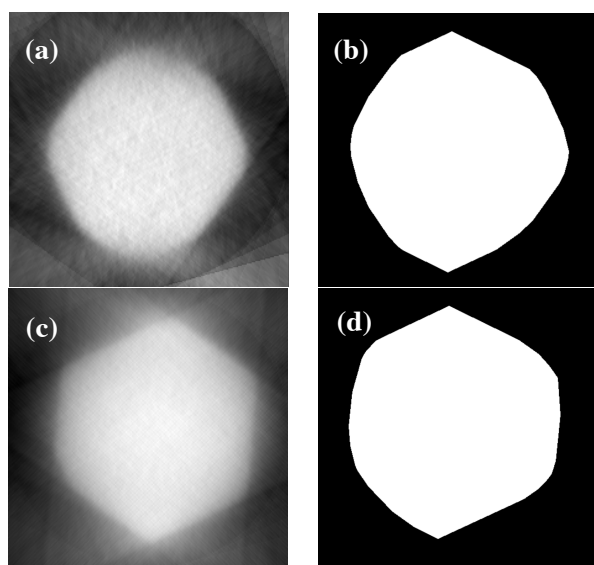


Figure 2. Reconstructed cross-sections from HAADF STEM tilt series using (a,c) SIRT and (b,d) GT algorithms from 14 equally-spaced projections over a tilt range of 139° . (a,b) are from the pale red line in Fig. 1, (c,d) from the dark blue line. Nanowire width is 140 nm measured from profiles in Fig. 1.

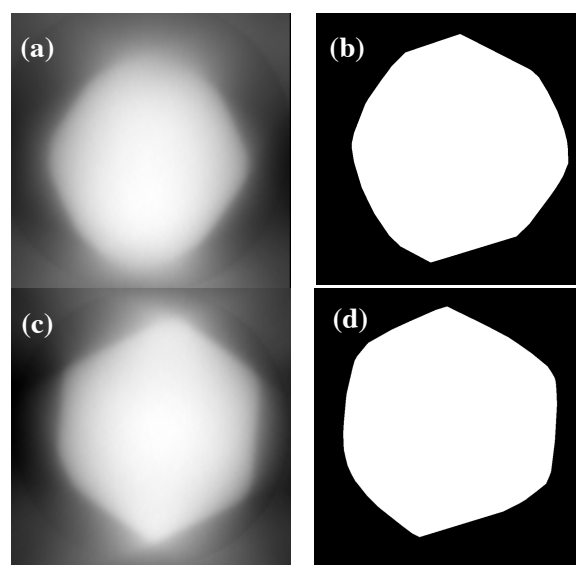


Figure 3. As Fig. 2, but reconstructed from 140 equally-spaced projections over a tilt range of 139° .

3. Geometric tomography from shadow outlines

The GT algorithm used in the present study, introduced by Gardner and Kiderlen [3], reconstructs only from the shadow outlines in each projection, neglecting any density variation. It is computationally simple: after thresholding, it fits a polygon to be consistent with the shadow outline from all projections. The algorithm used here converges as the number of projections approaches infinity [6]. Our implementation is more than an order of magnitude faster than SIRT [4,5]. Previous work has applied the GT concept to TEM images, but the back-projection algorithm used in [7] needs both post-reconstruction thresholding and is not proved to be convergent; the algorithm used in [8] is also not proved to be convergent. Our GT implementation [3] was applied to the same nanowire cross-sections (Fig. 1) that were used in section 2 after thresholding the input images at a value of 300 counts. For the present sample, our GT reconstructions from 14 and 140 projections are nearly identical, but the SIRT reconstructions improve with increased sampling. Our GT implementation and SIRT are in reasonable agreement outside the areas affected by the missing-wedge at the top and the bottom of the wire (Figs. 2, 3), where the SIRT reconstruction is blurred and our GT reconstruction is fully uninterpretable.

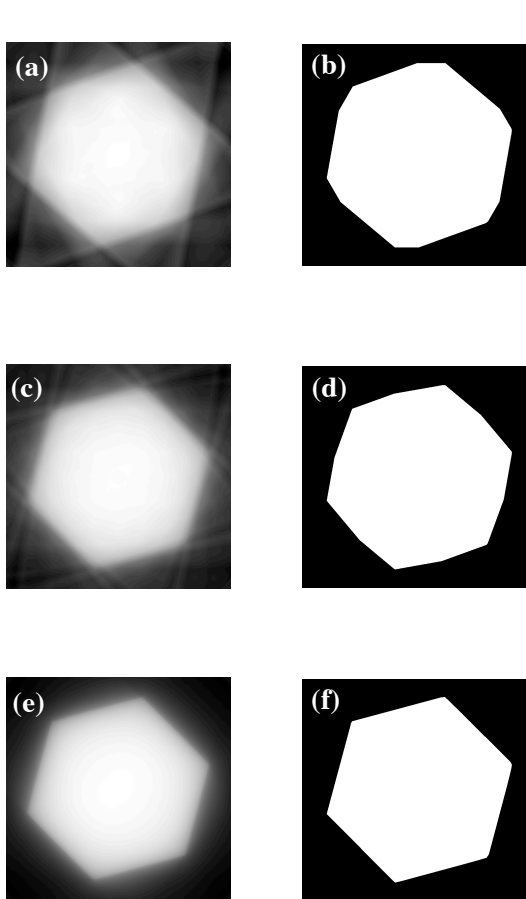


Figure 4. The effect of angular spacing on test data reconstruction for (a,c,e) SIRT and (b,d,f) geometric tomography for (a,b) 20°, (c,d) 10°, and (e,f) 1° with no noise and 180° tilt range.

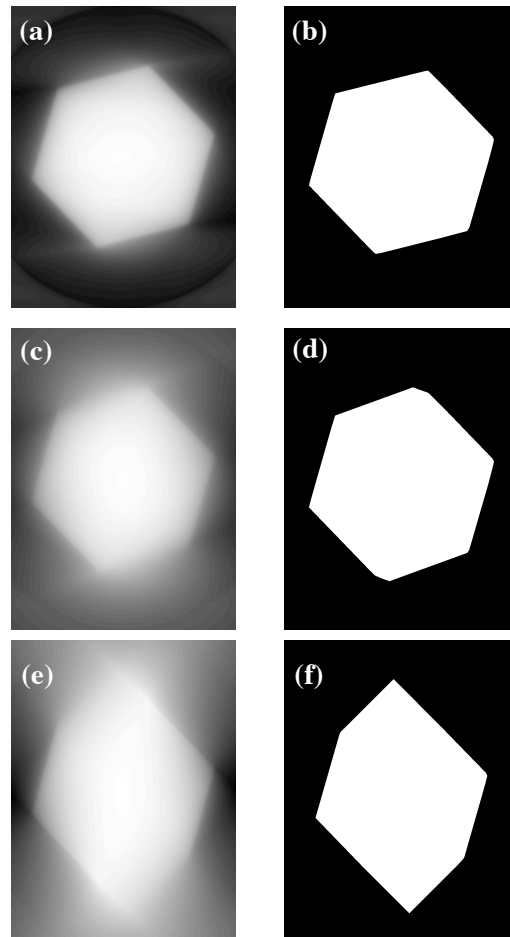


Figure 5. The effect of the missing wedge on test data reconstruction for (a,c,e) SIRT and (b,d,f) geometric tomography for (a,b) 160°, (c,d) 140°, and (e,f) 90° tilt range with no noise and 1° angular spacing.

4. Comparison of both geometric and algebraic algorithms using test data

To compare how individual factors affect this GT implementation and conventional SIRT, a simulated tilt series was generated from a regular, binary hexagon. The angular spacing between images (i.e. number of projections), tilt range and noise level were all individually varied, and image intensity fluctuations were used to simulate diffraction contrast.

Increasing the angular spacing creates artifacts outside the wire for the SIRT reconstruction, but a decrease in corner sharpness using GT (Fig. 4). Limiting the tilt range leads to missing-wedge effects in both algorithms, but the GT missing-wedge is more similar to the rest of the reconstruction (Fig. 5). The GT reconstruction can be sensitive to noise if it makes thresholding difficult, and this can lead to e.g. apparent facet artifacts. (Fig. 6), which may be a problem for the experimental GT reconstruction in section 3. For diffraction contrast, the SIRT reconstruction shows minimal change, but the GT reconstruction shows no change, because the model used here does not affect the outlines (Fig. 7).

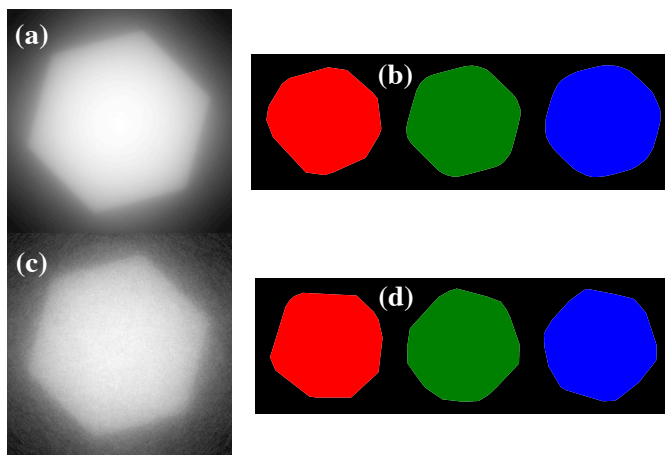


Figure 6. (a,c) SIRT and (b,d) GT reconstructions of the test hexagon with Gaussian noise level 10 \times (top) and 80 \times (bottom) the original intensity per object pixel. Color goes from red to green to blue (left to right) in (b,d) as the pre-reconstruction threshold T increases (b: $T=300,500,700$) (d: $T=2000,2700,2900$).

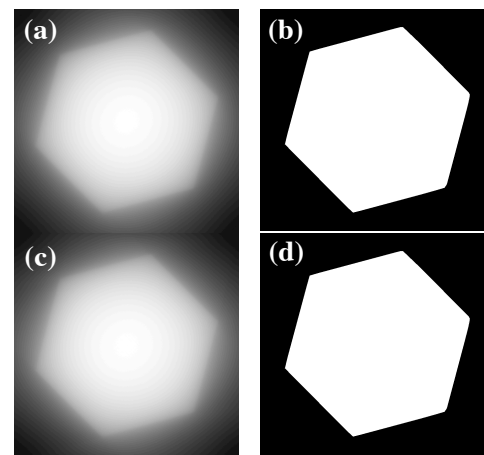


Figure 7. (a,c) SIRT and (b,d) GT reconstructions of the test hexagon for random diffraction contrast (50% chance of $\leq 25\%$ intensity increase (a,b) or $\leq 75\%$ intensity increase (c,d)).

5. Conclusions

A geometric tomography algorithm based on image outlines has been compared with algebraic tomography for an InAs nanowire with a convex cross-section. The missing wedge is a problem for both algorithms. Artifacts in the reconstruction may be more difficult to recognize for geometric tomography. Other geometric tomography algorithms can use the image intensity (e.g. [9]), instead of only the shadow outlines, potentially yielding a better reconstruction, especially in the missing-wedge region.

References

- [1] Herman G T 2009 *Fundamentals of Computerized Tomography*, (London: Springer)
- [2] Gardner R J 2006 *Geometric Tomography* (New York: Cambridge University Press)
- [3] Gardner R J and Kiderlen M 2009 *IEEE Trans. Pattern Anal. Machine Intell.* **31** 556-562
- [4] Abràmoff M D, Magalhães P J and Ram S J 2004 *Biophotonics International* **11** 36-43
- [5] Messaoudil C, Boudier T, Sanchez Sorzano CO and Marco S 2007 *BMC Bioinformatics* **8** 288
- [6] Gardner R J, Kiderlen M and Milanfar P 2006 *Ann. Statist.* **34** 1331-1374
- [7] Saghi Z, Xu X and Möbus G 2008 *Journal of Microscopy* **232** 186-195
- [8] Petersen T C and Ringer S P 2009 *J. Appl. Phys.* **105**, 103518
- [9] Gardner R J and Milanfar P 2003 *Discrete and Computational Geometry* **29** 279-303